PCCP

ROYAL SOCIETY OF CHEMISTRY

PAPER

View Article Online
View Journal | View Issue

Cite this: *Phys. Chem. Chem. Phys.*, 2024, **26**, 13875

Biophysical stimulation for bone regeneration using a chitosan/barium titanate ferroelectric composite

Razvan Rotaru, Violeta Melinte and Ioana-Sabina Trifan *

Received 2nd February 2024,
Accepted 16th April 2024

DOI: 10.1039/d4cp00497c

rsc.li/pccp

Herein we report the synthesis of a ferroelectric composed of chitosan (C)/barium titanate (BT) nanoparticles (NPs) with enhanced biocompatibility, non-toxicity, and piezoelectric behavior that can be advantageously used in biomedical applications. FTIR and SEM measurements were performed to assess the mechanism of interaction between the C matrix and BT NPs and their correlation with the biological responses. The dielectric measurements of the as-prepared composites reveal that incorporation of 50% BT NPs in the chitosan matrix leads to a steady increase of the dielectric constant as compared with neat chitosan films. The ferroelectric behavior of the sample was confirmed by the values of the loss factor (0.21–0.003) in the analyzed frequency range (10^{-1}–10^{6} Hz). This behavior suggests that ferroelectric C/BT nanocomposites can act as an active material that promotes accelerated bone regeneration.

1. Introduction

Ferroelectricity is the property of a specific class of electrical insulating materials that exhibit spontaneous electric polarization which may be reversed by applying an external electric field. All ferroelectrics are also piezoelectric (the external electric field is replaced by a field of mechanical forces – compression, stretching, torsion, *etc.*) and pyroelectric (the external electric field is replaced by a thermal field with a temperature different from that of the pyroelectric material), with the additional property that their natural electrical polarization is reversible. Since the discovery of ferroelectric ceramic materials (barium titanate, 1941)[1] these materials have become widely used in materials science and engineering applications as passive and active electronics components – ceramic condensers, multi-layer condensers, piezoelectric appliances, sensors, optical devices, thermistors, and electromagnets,[2–5] but biological and medical applications of these fascinating nanoparticles have only begun to be explored in the last two decades. For example, these materials can be used in a variety of ways: as imaging agents,[6] cell proliferation agents,[7] biocompatible nanoprobes,[8] and stimulation of bone healing.[9]

Barium titanate has the best ferroelectric properties (high polarization – over 8 μC cm^{-2}, high dielectric constant (about 8000) and low dielectric losses, lower than 0.1, at industrial frequency).[1,2] From the point of view of medical applications, barium titanate is non-toxic, but from the physical point of view it is obtained in the form of powder or by sintering in the form of hard ceramics.[1,2] For some medical applications, such as stimulating bone regeneration, it would be advantageous to use an elastic ferroelectric membrane. As barium titanate cannot be obtained in this form, the only solution would be to create a composite between a biocompatible polymer that can be obtained in the form of a membrane and the titanate powder to ensure the ferroelectric properties. Accordingly, Ciofani *et al.* prepared a ferroelectric poly(lactic-*co*-glycolic) acid/barium titanate composite for enhanced cellular proliferation.[10] Scalize and his colleagues prepared a poly(vinylidene fluoride-trifluoroethylene)/barium titanate membrane to trace the influence on human alveolar bone-derived cells,[11] while Vouilloz and his co-workers studied the reactivity of $BaTiO_3$–$Ca_{10}(PO_4)_6(OH)_2$ phases in composite materials for biomedical applications.[12]

Chitosan is an *N*-deacetylated product of chitin and the second most abundant natural polysaccharide (next to cellulose). Chitosan is embedded in a protein matrix of a crustacean shell or a squid pen.[13] For medical applications, chitosan has plenty of useful properties such as biocompatibility and biodegradability, wound healing properties, antimicrobial activity, antitumor effects, *etc.*[14,15] To produce homogeneous chitosan-based composite membranes, the polymer must be solubilized in a solution, ideally pure water in the case of bio applications. Chitosan, unfortunately, dissolves in strong acid solutions. Acidic solutions significantly altered the surface tension of chitosan solutions, which is critical for producing membranes by electrospinning or simple deposition. For example, membranes of

"Petru Poni" Institute of Macromolecular Chemistry of Romanian Academy, Romania. E-mail: trifan.sabina@icmpp.ro

chitosan nanofibers were prepared by electrospinning and chitosan was dissolved in concentrated acetic acid solution (90% acid concentration).[16] Homayoni and his colleagues advocate the hydrolysis of the polymer in NaOH (50%) for 8–48 hours at 95 °C and then the solubilization in acetic acid (70–90% concentration) for the advancement of the process of producing chitosan membranes.[17] Salazar-Brann *et al.*, using four types of acid (acetic acid, formic acid, lactic acid and citric acid), recommended concentrations of 90%.[18] However, the use of concentrated acid solutions might not be beneficial for some medical applications. In addition, optimal results in terms of mechanical properties are obtained when low concentrations of acid are used. Albanna *et al.* managed to improve the mechanical properties of chitosan-based heart valve scaffolds using chitosan fibers dissolved in 0.2 M acetic acid (1.2%) and stirring for 6 h.[19]

In terms of the medicinal use of ferroelectric composites, promoting bone regeneration is an intriguing yet essential concept that has received little attention. Due to the piezoelectric character of bone and the pyroelectric properties of collagen,[9,20,21] the presence of an electric or electromagnetic field recreates the growth (regeneration) microenvironment of bone tissue (stimulation and amplification of the deposition of Ca^{2+} ions in the form of calluses).[22] To produce electrical stimulation, three approaches are employed in practice: direct electrical stimulation (a) Fig. 1a, capacitive coupling (b) Fig. 1b, and the electromagnetic method (c) Fig. 1c. Direct electrical stimulation is a surgical procedure that requires the placement of two electrodes on the damaged bone. The supply current (continuous) has an intensity of 5–100 μA and a voltage of 1–10 V. The intensity of electric field obtained is 1–100 mV cm^{-1}. Capacitive coupling is a non-invasive approach that requires the direct connection of two planar capacitors to the skin in the area of the fracture and supply of a current of 1–10 V at frequencies of 20–200 kHz. The electric field generated is 1–100 mV cm^{-1}. The piezoelectric effect of ferroelectric materials that takes place during any mechanical action (movement, pushing, and bending) might substitute the electrical source when utilizing ferroelectric capacitors. The electromagnetic method uses two Helmholtz coils that can generate electromagnetic fields with the intensity of the electric component of 1–100 mV cm^{-1} and for the magnetic field component of 0.01–0.2 T. Until 2011, 105 direct clinical studies and 35 *in vitro* evaluations were done (studies known and reported to the "Oxford Center for Evidence Based Medicine"[23]). All studies have shown a reduction in the regeneration period of bone tissue. Side effects that have been reported may include the risk of infections and rejection reactions at the level of muscle tissue in the case of the direct electrical method (a) and adverse reactions (skin irritation) in the elderly in the case of methods (b) and (c). In the case of the capacitive method (b), the skin irritation is due to the heating of the capacitors during the direct supply of electric current. This heating would be reduced if ferroelectric capacitors were used. To the best of our knowledge, ferroelectric capacitors have never been tested.

The goal of this research is to create and analyze ferroelectric chitosan/barium titanate membrane composites that can be utilized to accelerate bone regeneration *via* capacitive coupling without a voltage source. A technique of chitosan solubilization with the least amount of acetic acid and a shorter processing time has also been studied.

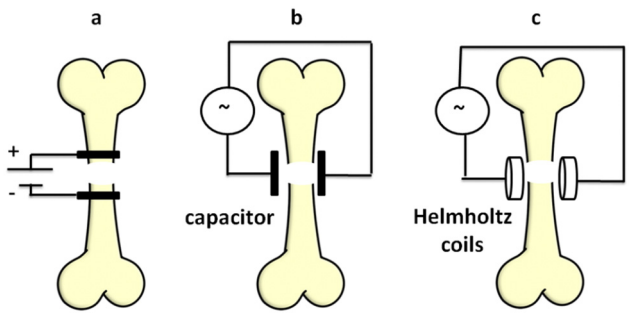

Fig. 1 Methods of electrical or electromagnetic stimulation of fracture regeneration (a: direct electrical stimulation, b: capacitive coupling, c: the electromagnetic method).

2. Experimental part

2.1. Materials

The materials used were chitosan (Aldrich, low molecular weight), glacial acetic acid (Aldrich, 99% purity), barium carbonate, titanium dioxide (Aldrich, 98% purity), and Milli-Q ultrapure distilled water (our laboratory).

2.2. Preparation of submicronic barium titanate particles

Barium titanate (BT) was prepared by using a modified solid state reaction under ultrasonic irradiation. The detailed procedure is described in a previous work.[2] Shortly, a 1 : 2 titanium dioxide/barium carbonate (w/w) mixture was ultrasonically irradiated at 20 kHz frequency, in Milli-Q ultrapure water for 60 min by using a Sonics Vibracell generator (750 W electric power converted in ultrasound waves) equipped with a probe and sensor for temperature. The obtained powder was further decanted and dried in a microwave furnace for 10 min. The last treatment involved a heating process for 3 h, undertaken in a furnace at 500 °C to obtain perovskite-like BT particles of submicronic dimensions (400–600 nm). The modified method improved the efficiency of the energy, as well as the synthesis time compared to the classic solid state reaction method.[2,24–27]

2.3. Preparation of chitosan membranes

Three initiatives were made to directly dissolve chitosan powder (C) in water using ultrasonic irradiation for 10, 20, and 30 minutes, respectively. From a quantitative standpoint, 1 gram of chitosan (C) and 60 ml of Milli-Q water were employed. An amount of 60 ml of water was chosen according to the studies of previous works[28,29] as optimal, in relation to the technical requirements of the ultrasound generator used (the ultrasound probe should be immersed in a liquid medium at least 40% of its length and the distance between it and the walls of the glass should be as small as possible). After ultrasonication, the samples are poured into a Petri dish and left in

Table 1 Sample codes and preparation conditions for chitosan membrane synthesis

Sample	Ultra-sonication medium	Ultrasonic time-span [min]	Dissipated energy [kJ]	T_{max} (ultra-sonication) [°C]
C_{a10}	Water	10	24.5	84
C_{a20}	Water	20	40.3	85
C_{a30}	Water	30	63.5	87
C_{b15}	Acetic acid 3.33%	15	35.4	94

a ventilated oven at a temperature of 50 °C for 24 hours. The chitosan powder is partially, not completely, dissolved during ultrasonication and the membranes obtained are non-transparent, white and brittle. Another membrane was obtained using a glacial acetic acid solution of 3.33% concentration. Specifically, 1 g of C, 2 ml of acetic acid and 58 ml of Milli-Q water were used. In this case, 15 minutes of ultrasonication are sufficient to obtain complete dissolution. As in the previous cases, the solution of chitosan in diluted acetic acid was poured into a Petri dish and left in the ventilation oven at 50 °C for 24 h. A slightly yellowish transparent membrane with good mechanical elasticity properties is obtained. Membrane codes and synthesis terms are shown in Table 1.

2.4. Preparation of chitosan/barium titanate based membranes

For the preparation of composite membranes with ferroelectric BT, the option of solubilization in weakly concentrated acetic acid (3.33%) was chosen in order to obtain films with good mechanical properties. Three quantitative percentages were chosen for the ratios between C and BT, C/BT, of 1/0.1, 1/0.25 and 1/0.5, respectively. The steps of the synthesis were followed from obtaining the chitosan membrane in diluted acetic acid. Specifically, 1 g of C, 0.1, 0.25 and 0.5 g of BT are used and ultrasonicated for 15 minutes in 58 ml of Mill-Q water and 2 ml of acetic acid. After drying in the oven with ventilation, non-transparent, yellow–white membranes with good mechanical properties are obtained. Composite membrane codes and synthesis terms are shown in Table 2.

2.5. Methods

The chemical structures of all membrane samples, along with commercial chitosan and $BaTiO_3$, were investigated by Fourier-transform infrared (FTIR) spectroscopy in the attenuated total reflectance (ATR) method using a Shimadzu IRAffinity-1S spectrophotometer with 32 scans and resolution of 4 cm^{-1} to record the transmittance spectra in the range of 4000–400 cm^{-1}. X-ray diffraction analysis for barium titanate was performed on a Bruker Advance D8 X-ray diffractometer (λ: 0.15405 nm – the wavelength of Cu Kα1 radiation, 2θ from 5 to 50 degrees-angular region). Scanning electron microscopy surface morphology images were acquired by using a Verios G4 UC scanning electron microscope (Thermo Fisher Scientific) provided with an energy dispersive spectrometer (EDS, EDAX Octane Elite). For the analysis in the cross-section of the composite samples, these were fractured by freezing in liquid nitrogen, and the broken surface of the films was sputter-coated with a thin layer of platinum to increase visualization of the composite morphology. The dielectric measurements were performed on a Concept 40 Novocontrol dielectric spectrometer at room temperature, with silver electrodes, in the 10^{-1}–10^{6} Hz frequency range. The contact surfaces with spectrometer electrodes were covered with silver conductive paste to avoid interfacial polarization and possible edge effects. The sample of BT powder was prepared as cylindrical pellets (13 mm diameter, 3 mm thickness) using a Specac laboratory press (10 ton pressure).

To calculate the intensity of the electric field at the level of the fractured bone, the following formulae and assumptions were used:[30]

$$E = \frac{Q}{4\pi\varepsilon_h r^2} \quad (1)$$

$$Q = C \cdot V \quad (2)$$

$$C = \frac{\varepsilon \cdot S}{d} \quad (3)$$

where

- E is the intensity of the electric field emitted by the composite membrane at the level of the fractured bone;
- Q is the electric charge stored by the composite membrane;
- π = 3.1415;
- ε_h: the dielectric constant of human skin and tissue that separates the free medium from bone, $\varepsilon_h \sim 500$;[31]
- r: skin and tissue thickness, $r \sim 5$ mm;
- C is the electrical capacity of the capacitor formed by the composite membrane;
- V is the electric potential difference used to charge the capacitor, V = 220 V, the membrane is directly charged at 220 volts before contact with human skin;

Table 2 Sample codes and preparation conditions for chitosan/barium titanate composite synthesis

Sample	Chitosan/$BaTiO_3$ w/w	Ultra-sonication medium	Ultrasonic time-span [min]	Dissipated energy [kJ]	T_{max} (ultra-sonication) [°C]
C/BT_1	1/0.1	Acetic acid 3.33%	15	37.5	95
$C/BT_{2.5}$	1/0.25	Acetic acid 3.33%	15	37.8	96
C/BT_5	1/0.5	Acetic acid 3.33%	15	37.9	96

- ε: dielectric constant of the composite membrane, the value is chosen from industrial frequencies (50–55 Hz), taking into account that the electric charge is made at 220 V, the same frequency;

- S: the surface of the composite membrane, $S = 132.72$ mm^2, the ferroelectric membrane is circular with a radius of 6.5 mm;

- d: the thickness of the composite membrane, $d = 2$ mm.

The mechanical parameters (tensile strength, elongation at break, Young's modulus and toughness) of the chitosan film (C_{b15}) and of the composites (C/BT$_1$, C/BT$_{2.5}$ and C/BT$_5$) were determined on a Shimadzu AGS-J deformation apparatus at ambient temperature. The samples were cut into rectangular specimens (25 mm × 5 mm × 0.3 mm), the initial grip separation was set at 25 mm and the cross-head speed was set at 1 mm min^{-1}. This test was repeated 3 times for each specimen in order to confirm its repeatability and the average values were taken.

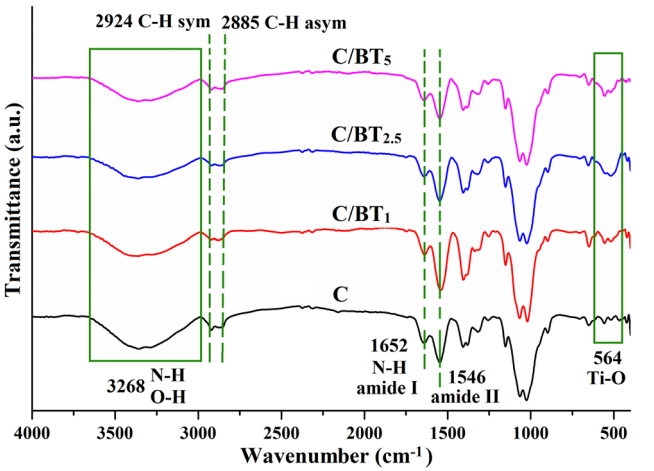

Fig. 3 ATR–FTIR spectra of chitosan based-composite membranes.

3. Results and discussion

3.1. Fourier-transform infrared (FTIR) spectroscopy and XRD analysis

X-ray powder diffraction (XRD) analysis was used to accomplish a deeper structural characterization of the barium titanate thus checking the purity but also the crystalline structure (the cubic structure of barium titanate being paraelectric and the tetragonal or hexagonal one being ferroelectric). The X-ray diffraction pattern for BT is depicted in Fig. 2a.

Barium titanate diffractograms present signals at 22.2°, 31.6°, 39° and 45.4° assigned to (100), (101), (111) and (200) specific to pure barium titanate according to JCPDS, without traces of any detectable impurities. On Miller planes (100) and (200) there are two splits at 22° and 45.1°, respectively, assigned to planes (001) and (002). These splitting are specific only to barium titanate with a tetragonal crystal structure, and therefore ferroelectric.[2,32] As observed from Fig. 2b, the infrared spectrum of the BT sample shows characteristic bands for pure barium titanate at 438 cm^{-1} and 559 cm^{-1}.[2] The band observed at lower wavenumbers is one of the 'fingerprints' of barium titanate and it is attributed to the Ba–O and Ti–O metal oxide vibration.[2,33] In the case of composites with BT nanoparticles (Fig. 3), the Ti–O$_I$ stretching band shift at a higher value of the wavenumber is very important because it suggests the formation of $BaTiO_3$ tetragonal phase thus confirming the X-ray diffraction analysis.[2,34] Besides, these shifts may appear as a result of ultrasonication. However, other small bands appear at 1425 cm^{-1} and may also be a consequence of the previous ultrasonication and around 1400–1600 cm^{-1} as intrinsic signals for Ti–O.[35] The visible changes in the intensity of the Ti–O corresponding band at 564 cm^{-1} can be justified by the structural modification that may interfere with both of $BaTiO_3$ and chitosan matrix during synthesis, as well as by the possibly reduced aggregation of inorganic nanoparticles that may lead to its decrease.[36] Aggregation of BT nanoparticles into the chitosan matrix may occur as a consequence of electrostatic

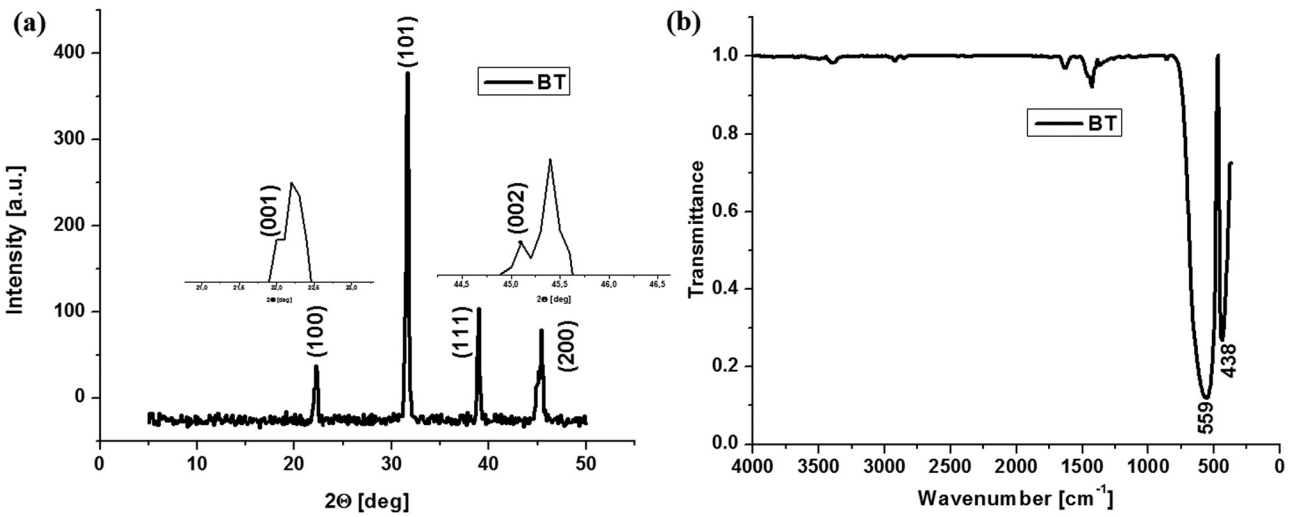

Fig. 2 XRD diffraction of BT (a) and FTIR spectrum of BT (b).

interaction formation after being polarized under an applied field.[37]

In Fig. 3, the characteristic bands of chitosan appear at 3268 cm^{-1} and 1667 cm^{-1} corresponding to the N–H stretching vibration from the amine and amide groups in the polysaccharide backbone, while the stretching bands for C–H of the repeating units appear at 2924 cm^{-1} (symmetric) and 2885 cm^{-1} (asymmetric). The band assigned to O–H stretching vibration overlaps with the one of N–H at 3268 cm^{-1}. The bands corresponding to amide I (C═O stretching vibration) and amide II (N–H bending and C–N stretching) also appear at 1635 cm^{-1} and 1545 cm^{-1}.[38] The spectra of membranes containing BT ferroelectric particles have bands characteristic of BT, along with those attributed to chitosan. Fig. 3 also highlights the band at 564 cm^{-1}, attributed to Ti–O and specific to all hybrid composites, proving the incorporation of BT particles into the polymeric matrix of chitosan. As expected, this band appears to be broader and increased for the membranes having a higher amount of BT particles included ($C/BT_{2.5}$ and C/BT_5). Besides, the mixture between inorganic and organic compounds is required to be homogenous in order to form heterojunctions between the phases, which implies a good stress distribution within the entire composite surface. The band assigned to O–H stretching vibration overlaps with the one of N–H at 3268 cm^{-1}.[38,39] The bands corresponding to amide I (C═O stretching vibration) and amide II (–NH bending and C–N stretching) also appear at 1635 and 1545 cm^{-1}.[38] The spectra of membranes containing BT ferroelectric particles have bands characteristic of BT, along with those attributed to chitosan. Fig. 3 also highlights the band at 564 cm^{-1}, attributed to Ti–O and specific to all hybrid composites, proving the incorporation of BT particles into the polymeric matrix of chitosan. As expected, this band appears to be broader and increased for the membranes having a higher amount of BT particles included ($C/BT_{2.5}$ and C/BT_5).

3.2. Morphology investigation

The fracture morphology of the chitosan film and of its composites with barium titanate was investigated by scanning electron microscopy (SEM), the selected images at two magnifications (5000× and 20 000×) being included in Fig. 4.

As can be observed in Fig. 4a and b, the morphology of the Cb_{15} membrane is characterized by a compact, homogeneous structure without visible voids. The inclusion of BT in the chitosan matrix is evidenced by the presence of small white particles, uniformly distributed in the organic template. At lower BT contents, the particles are better covered with chitosan, simultaneously evidencing the formation of some elongated pores that accommodate the inorganic BT particles, while the formation of clearer and sharper fracture edges indicates the strengthening of the chitosan organic matrix. At higher loadings (*e.g.* for C/BT_5 Fig. 4g and h), the increasing number of BT particles connected only by weak interaction with the chitosan phase determines the formation of some small particle clusters, although the overall distribution of the particles in the chitosan template seems homogeneous.

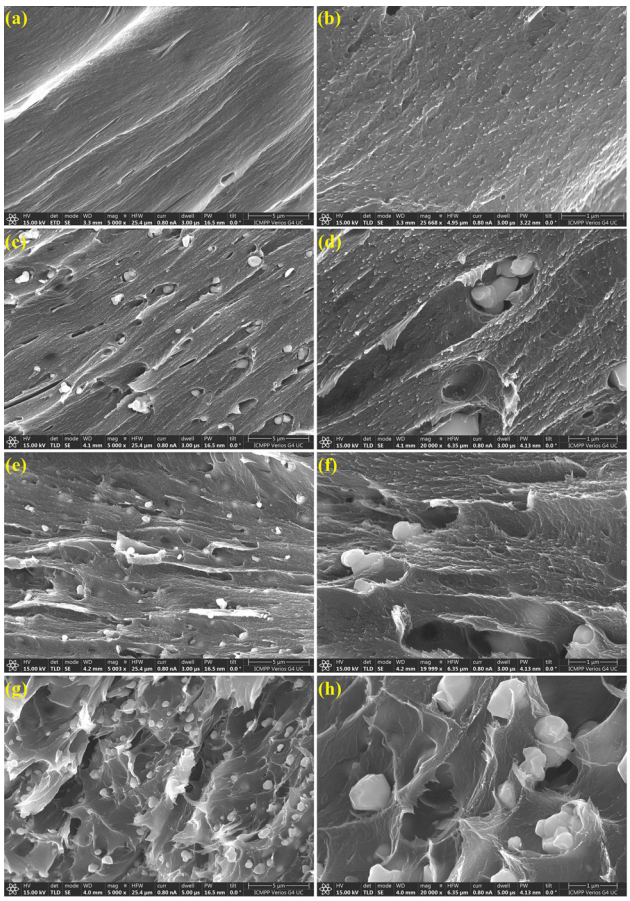

Fig. 4 SEM images of chitosan C_{b15} (a) and (b), C/BT_1 (c) and (d), $C/BT_{2.5}$ (e) and (f) and C/BT_5 (g) and (h) samples in cryo-fractured sections.

These clusters determine the formation of some micro-voids and defects inside the membrane structure, which potentially may result in changes in the mechanical strength of the composite material, although the structural integrity of the C/BT_5 film is very well preserved.

3.3. Dielectric properties

The components of the complex dielectric permittivity (dielectric constant, ε' and absorption or loss permittivity, ε'') were measured in the frequency range of 10^{-1}–10^{6} Hz at room temperature. The dielectric constant and dielectric losses specific for insulating materials (such as chitosan and barium titanate) are attributed to the polarization of the electrons and molecules, which includes five types of polarization: electronic, vibrational (or atomic), orientation (or dipolar), ionic and interfacial polarization. Electronic and vibrational polarizations are ideal for materials used like capacitors because they have small dielectric losses while the ionic and interfacial polarizations result in high dielectric losses and they inherently have long discharge times (which is an advantage for stimulating bone regeneration through the capacitive coupling method). For ferroelectric materials ε' show high values and ε'' show small values compared with the dielectric constant so that the ratio $\varepsilon''/\varepsilon'$, also called the tangent of the loss angle

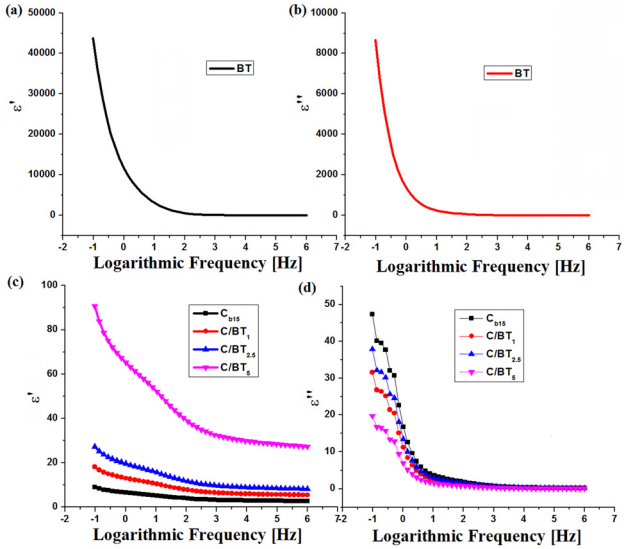

Fig. 5 Dispersion ($\varepsilon' = \varepsilon'(\nu)$) and absorption ($\varepsilon'' = \varepsilon''(\nu)$) spectra for BT (a) and (b) and chitosan membrane (C_{b15}) and C/BT composites (c) and (d) respectively.

(tg δ), has subunit values at any frequency (below 0.3 for any frequency range analyzed).[2] The variation ε' and ε'' as a function of frequency for barium titanate depicted in Fig. 5a and b and for chitosan membrane and chitosan/barium titanate in Fig. 5c and d. The variation of the loss factor (tg $\delta = \varepsilon''/\varepsilon'$) is shown in Fig. 6.

For BT, as one may see from Fig. 5a and b, with frequency, ε' and ε'' decrease and remain constant at higher frequencies indicating the occurrence of dielectric dispersion (ionic and orientation polarizabilities). This may be attributed to the dipoles resulting from changes in valence states of cations and space-charge polarization.[2,40] The decrease in the value of the dielectric constant starts from frequencies higher than 100 Hz. Electronic polarization (corresponding to ε') is always

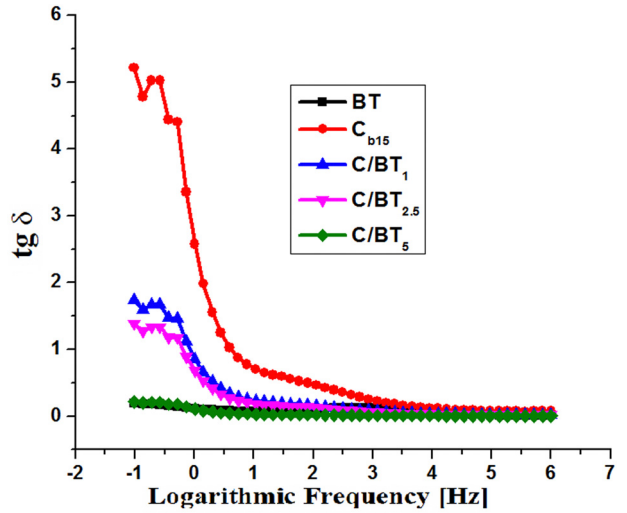

Fig. 6 The variation of the tangent of the loss angle for BT, the chitosan membrane and the composites with barium titanate.

higher than ionic and orientation polarization (corresponding to ε'') at any frequency. This is a normal behavior for ferroelectric materials.[41] ε' ranges from 14 for 10^6 Hz up to 43 600 for 10^{-1} Hz while ε'' registers values from 0.05 for 10^6 Hz up to 8654 for 10^{-1} Hz.

As far as chitosan is concerned, it presents for dielectric permittivity values a normal variation for insulating materials without ferroelectric properties. ε' takes values from 2.7 at high frequencies (10^6) to 9 at low frequencies (10^{-1}) and ε'' varies from 0.2 to 47.3 for the same frequency range. A chitosan capacitor subjected to an electric potential difference will retain a limited amount of energy (proportional to ε') and will release it very quickly in the form of an electric field in the near external environment, unlike ferroelectric material capacitors that release energy over long time. Barium titanate composites behave differently. The dielectric constant ε' undergoes a value increase compared to that of the chitosan membrane. Thus, in the interval 10^{-1}–10^6, ε' takes values between 5.4 and 18.1 for the C/BT1 composite, between 8.1 and 27.2 for $C/BT_{2.5}$, respectively between 27.2 and 90.7 for C/BT_5. In the same frequency interval analyzed, ε'' take values between 0.1 and 31.5 for C/BT_1, between 0.1 and 37.8 for $C/BT_{2.5}$, respectively 0.08 and 19.7 for C/BT_5. Another characteristic of ferroelectric materials is the subunitary value of the tangent of the loss angle (tg $\delta = \varepsilon''/\varepsilon'$). It actually represents the ratio between the energy taken by the ferroelectric material from the outside and transformed into heat and the energy stored in the material and given to the external environment in the form of an electric field in a relatively large time interval. Fig. 6 shows the variation of the tangent of the loss angle for BT, the chitosan membrane and the composites with barium titanate.

In the case of barium titanate, the loss factor takes values between 0.19 and 0.003 in the analyzed frequency range (10^{-1}–10^6 Hz). These values are specific to ferroelectric materials. In the same frequency range, the loss factor for the chitosan membrane takes values from 5.21 to 0.07. They are characteristic values of an electrical insulating material without ferroelectric properties. As for the C/BT composite membranes, they behave differently depending on the amount of incorporated barium titanate. Thus C/BT_1 and $C/BT_{2.5}$ behave more like a chitosan membrane, the loss factor having values between 1.73 and 0.02 (for 10% BT) and between 1.39 and 0.01 (for 25% BT). The amount of 10% or 25% of BT embedded in the chitosan membrane does not ensure ferroelectric properties at the composite level. In the case of the C/BT_5 composite (50% BT ratio), the loss factor takes values between 0.21 and 0.003, almost like the values measured in the case of pure barium titanate. Thus it can be said that the C/BT_5 composite has ferroelectric properties and can be used as such.

Fig. 7 shows the variations in the intensity of the electric field emitted by the composite membranes at the level of the fractured bone, calculated using formulas (1)–(3).

C/BT_1 and $C/BT_{2.5}$ membranes emit electric fields below 10 mV cm^{-1}. A large part of the charging energy of the capacitor formed with these membranes is transformed into heat, not into an electric field, and in addition, due to the predominantly non-ferroelectric character (high tg δ), the electric discharge is

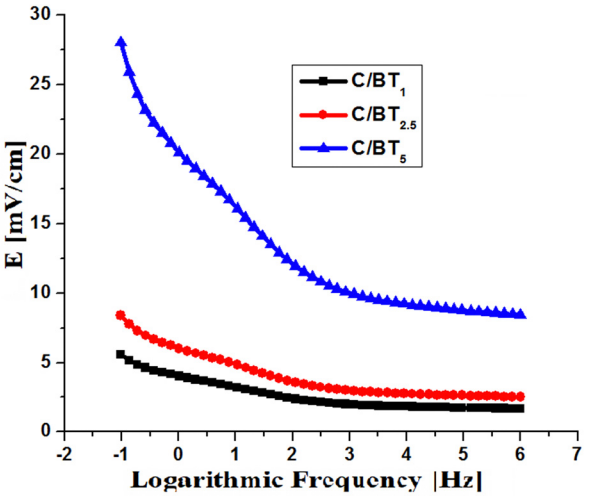

Fig. 7 The intensity of the electric field emitted by the composite membranes at the level of the fractured bone.

done in a short time. The C/BT_5 membrane (with 50% BT) emits electric fields with values between 8.3 (at high frequencies) and 28 mV cm^{-1} (at low frequencies). Due to the ferroelectric character (subunit $tg\,\delta$ at any frequency) the electric field emission will last over time, making direct connection to a permanent power supply no longer necessary. For the practical case of charging at a 220 V power source at industrial frequencies (a simple alternating current socket), the intensity of the emitted electric field is 14 mV cm^{-1}.

Table 3 presents a comparison between the dielectric constants of some materials used in the medical field and the chitosan/barium titanate membranes described in this work.

3.4. Mechanical properties

For the envisaged applications, the mechanical behaviour of chitosan films and of the prepared composites represents a critical parameter, reason for that their tensile strength and elongation properties were investigated and the achieved results are included in Fig. 8. The stress–strain graphs illustrated in Fig. 8a indicated that pristine chitosan display good mechanical characteristics with an elongation at break of 11.18% and a maximum tensile strength of 47 MPa, characteristics that suffer some modification by the inclusion of barium titanate particles.

Thus, for the sample C/BT_1, the incorporation of 10 wt% BT determines a small adjustment of the elongation and tensile strength, while the embedding of 25 wt% BT in $C/BT_{2.5}$ membrane induced an enhancement of maximum stress to 59 MPa and a reduction almost to half of the elongation. The further augmentation of BT percent in C/BT_5 sample has as a result a diminish of the mechanical parameters (maximum tensile stress and elongation at break) as compared to $C/BT_{2.5}$ sample, suggesting that an enhanced amount of BT particles could affect the cohesion of chitosan macromolecular chains.

However, from Fig. 8b it can be observed that the progressive enhancement of the BT amount in the chitosan membranes determines a significant improvement of Young modulus values (from 0.65 GPa in Cb_{15} to 2.24 GPa in C/BT_5), indicating, as expected, an increase of the films stiffness. Toughness, defined as the capacity of a material to absorb energy and plastically deform without fracturing, is given by the area under the stress–strain curves and varied for the investigated films between 0.4 MJ m^{-3} for Cb_{15} sample and 0.21 MJ m^{-3} for C/BT_5 membrane. The reduction in toughness to nearly half caused by the presence of BT particles can be associated with Young modulus values, confirming the rise in the rigidity of the C/BT_5 film. This is a typical behavior for hybrid materials, as the polymeric components provide flexibility to the composite while their inorganic counterparts, $BaTiO_3$ particles in our case, induced a strength enhancement.[51–53] The improvement of the mechanical properties for composites is conditioned by the uniform distribution of the inorganic phase in the organic matrix, which promotes the interfacial surface interactions while simultaneously optimizing the organic–inorganic interactions. Recent studies have demonstrated that surface modification of nanometer-sized $BaTiO_3$ NPs[54] and large diminish of the nanoparticles amount up to 9 wt%[55] lead to chitosan/$BaTiO_3$ composites with reduced agglomeration. For the materials proposed in this study, increasing the BT loading level results in a gradual enhancement of Young's modulus, concomitant with a decrease of elongation at break, confirming the reinforcing effect of inorganic nanoparticles corroborated with some wick polymer/filler interfacial interactions that enhance the strength of the films in detriment of ductility. It is evident that the incorporation of significant higher amounts of BT particles (around 50 wt%) inside the chitosan membranes determine a lowering of interfacial adhesion between

Table 3 Materials use for orthopedic implants, adhesion, growth and enzymatic activity of human osteoblast, bone regeneration

Materials	ε'	Key assessments	Ref.
$(Na_{0.5}K_{0.5})NbO_3$	657	Orthopedic implants	42
$LiNbO_3$	62	Adhesion growth enzymatic activity of human osteoblast	42
$KNbO_3$	394	Orthopedic implants biomineralization osteoblast cell proliferation	43
ZnO	12	Orthopedic implants	44
Polyvinylidene fluoride	—	Orthopedic implants	45
Chitosan	4	Orthopedic implants	46
Barium titanate/graphene/poly-L-lactic acid	—	Improves piezoelectric performance of biopolymer scaffold	47
Graphene oxide/polyvinylidene fluoride	—	Reconstruction of electrical microenvironment of bone tissue	48
Core shell barium titanare carbon/polyvinylidene fluoride	—	Bone healing	49
Barium titanate/titanium	—	Bone defects	50
Chitosan/barium titanate (C/BT_5)	27–91	Bone regeneration	This work

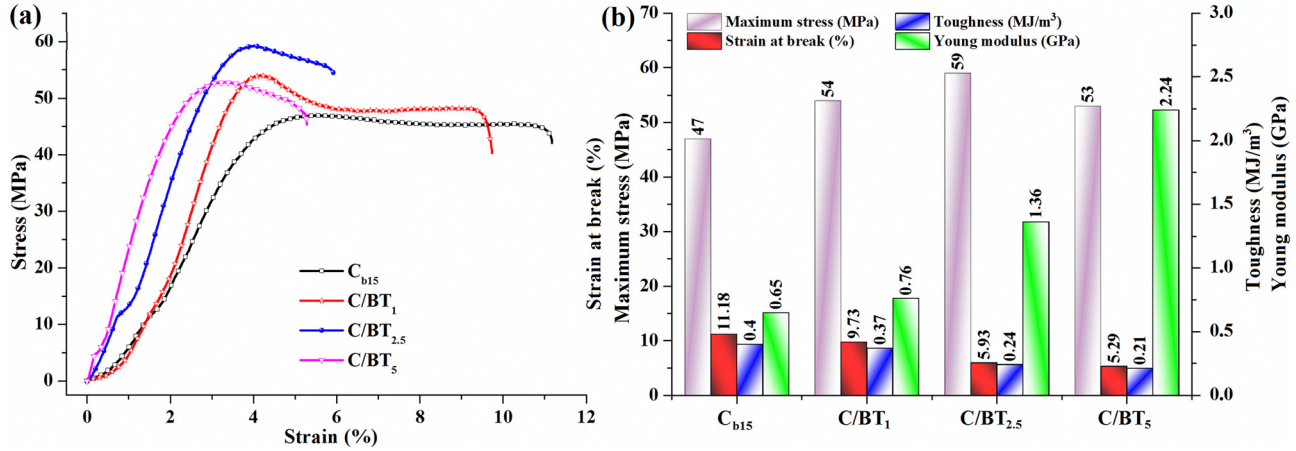

Fig. 8 Tensile stress–strain curves of the chitosan based membranes (a) and variation of mechanical parameters (maximum stress, strain at break, toughness and Young's modulus) as a function of composition of the samples (b).

the organic and inorganic phases, and some agglomeration phenomena are likely to occur, as observed also from the fractured surfaces. However, in accord with similar materials reported in the literature,[56] the favourable mechanical features (tensile strength and elastic modulus) of the investigated chitosan/BT composites recommend their utilization as scaffolds for bone tissue engineering.

Conclusions

In this work, enhanced piezoelectric and biocompatibility properties of C/BT nanocomposites films with different amount of BT NPs has been investigated. Also, BT NPs demonstrate ferroelectric and piezoelectric properties. Moreover BT NPs demonstrate good dispersion in C matrix up to 35 wt% of NPs. Therefore, investigated C/BT piezoelectric nanocomposites could act as a biochemical platform to accelerate bone regeneration *via* capacitive coupling without a voltage source, with potential applications in injured bone remediation due to flexibility and biocompatibility of C/BT nanocomposite films.

Author contributions

Conceptualization, I.-S. T. and R. R.; methodology, R. R.; validation, R. R. and I.-S. T.; formal analysis, R. R., V. M., and I.-S. T.; investigation, R. R., and I.-S. T.; resources, R. R., I.-S. T. and V. M.; writing – original draft preparation, R. R.; writing – review and editing, R. R., I.-S. T. and V. M.; visualization, I.-S. T., V. M.; supervision, R. R., I.-S. T. All authors have read and agreed to the published version of the manuscript.

Conflicts of interest

There are interests to declare.

References

1 S. Gupta, *Electron. Opt. Mater.*, 2021, 1–41.
2 R. Rotaru, C. Peptu, P. Samoila and V. Harabagiu, *J. Am. Ceram. Soc.*, 2017, **100**(10), 4511–4518.
3 R. Rotaru, C. Peptu and V. Harabagiu, *Cellul. Chem. Technol.*, 2016, **50**(5–6), 621–628.
4 M. E. Culica, G. Biliuta, R. Rotaru, G. Lisa, R. I. Baron and S. Coseri, *Polym. Eng. Sci.*, 2019, **59**(7), 1499–1506.
5 R. Rotaru, C. M. Popescu, A. Dascalu, D. Timpu, M. Asandulesa, M. E. Fortuna and V. Harabagiu, *Rev. Roum. Chim.*, 2023, **68**(3–4), 175–185.
6 S. Coseri, A. Spatareanu, L. Sacarescu, V. Socoliuc, I. S. Stratulat and V. Harabagiu, *J. Appl. Polym. Sci.*, 2016, **133**(5), 42926.
7 W. Wang, J. Li, H. Liu and S. Ge, *Adv. Sci.*, 2021, **8**(1), 2003074.
8 A. Sood, M. Desseigne, A. Dev, L. Maurizi, A. Kumar, N. Millot and S. S. Han, *Nano Micro Small*, 2022, **19**(12), 2206401.
9 C. Yang, J. Ji, Y. Lv, Z. Li and D. Luo, *Nanomaterials*, 2022, **12**(24), 4386.
10 G. Ciofani, L. Ricotti, A. Menciassi and V. Mattoli, *Biomed. Microdevices*, 2011, **13**, 255–266.
11 P. H. Scalize, K. F. Bombonato-Prado, L. Gustavo de Sousa, A. L. Rosa, M. M. Beloti, M. Semprini, R. Gimenes, A. L. G. de Almeida, F. Singaretti de Oliveira, S. C. H. Regalo and S. Siessere, *Tissue Engineering Constructs and Cell Substrates*, 2016, **27**(12), 180.
12 F. J. Vouilloz, M. S. Castro, G. E. Vargas, A. Gorustovich and M. A. Fanovich, *Ceram. Int.*, 2016, **43**(5), 4212–4221.
13 I. A. Duceac and S. Coseri, *Biotechnol. Adv.*, 2022, **61**, 108056.
14 F. Zhang, S. Zhang, R. Lin, S. Cui, X. Jing and S. Coseri, *Int. J. Biol. Macromol.*, 2023, **249**, 125801.
15 I. A. Duceac, L. Vereştiuc, A. Coroaba, D. Arotăriţei and S. Coseri, *Int. J. Biol. Macromol.*, 2021, **181**, 1047–1062.
16 A. Pérez-Nava, E. Reyes-Mercado and J. Betzabe González-Campos, *Chem. Eng. Process.*, 2022, **173**, 108849.

17 H. Homayoni, S. A. H. Ravandi and M. Valizadeh, *Carbohydr. Polym.*, 2009, **77**, 656–661.
18 S. A. Salazar-Brann, R. Patiño-Herrera, J. Navarrete-Damián and J. F. Louvier-Hernández, *AIMS Bioeng.*, 2021, **8**(1), 112–129.
19 M. Z. Albanna, T. H. Bou-Akl, H. L. Walters III and H. W. T. Matthew, *J. Mech. Behav. Biomed. Mater.*, 2012, **5**, 171–180.
20 J. C. Anderson and C. Erikson, *Nature*, 1968, **218**, 166–168.
21 S. Cui, S. Zhang and S. Coseri, *Carbohydr. Polym.*, 2023, **300**(11), 120243.
22 L. Leppik, K. M. C. Oliveira, M. B. Bhavsar and J. H. Barker, *Eur. J. Trauma Emerg. Surg.*, 2020, **46**(2), 231–244.
23 M. Griffin and A. Bayat, *J. Plast. Surg.*, 2011, **11**, 303–353.
24 J. L. C. Huamán, J. C. Sczancoski, E. Marega Jr. and A. H. Pinto, *Recent Advances and Emerging Applications, Advanced Ceramic Materials*, 2023, 31–75.
25 J. L. C. Huamán, G. Nicolodelli, G. Lozano C, V. A. G. Rivera, S. O. Ferreira, A. H. Pinto, M. S. Li and E. Marega Jr., *Phys. Chem. Chem. Phys.*, 2021, **23**, 18694.
26 J. L. C. Huamán, N. A. Baharuddin, M. A. Mohamed, A. A. Samat, H. A. Rahman and E. Marega Jr., *Adv. Ceram.*, 2024, 47–112.
27 J. L. C. Huamán and V. A. G. Rivera, *Perovskite Ceramics, Advanced Ceramic Materials*, 2023.
28 R. Rotaru, P. Samoila, N. Lupu, M. Grigoras and V. Harabagiu, *Rev. Roum. Chim.*, 2017, **62**(2), 131–138.
29 R. Rotaru, M. Savin, N. Tudorachi, C. Peptu, P. Samoila, L. Sacarescu and V. Harabagiu, *Polym. Chem.*, 2018, **9**, 860–868.
30 E. M. Purcell, *Electricity and Magnetism. Berkeley Physics Course*, McGraw-Hill, New York, 1984, p. 2.
31 S. Huclova, D. Erni and J. Fröhlich, *J. Phys. D: Appl. Phys.*, 2012, **45**, 025301.
32 A. E. Hassanien, T. Matar, A. F. Mabied, A. A. Ramadan and H. M. Hashem, *Egypt. J. Chem.*, 2023, **66**(8), 67–71.
33 A. F. Suzana, S. Liu, J. Diao, L. Wu, T. A. Assefa, M. Abeykoon, R. Harder, W. Cha, E. S. Bozin and I. K. Robinson, *Adv. Funct. Mater.*, 2023, **33**(19), 2208012.
34 M. Tihtih, J. E. F. M. Ibrahim, M. A. Basyooni, R. En-nadir, W. Belaid, I. Hussainova and I. Kocserha, *ACS Omega*, 2023, **8**(9), 8448–8460.
35 M. Reda, S. I. El-Dek and M. M. Arman, *J. Mater. Sci.: Mater. Electron.*, 2022, **33**, 16753–16776.
36 S. H. Lee, Y. C. Choi, K. M. Ryu and Y. G. Jeong, *Fibers Polym.*, 2020, **21**, 473–479.
37 L.-X. Gao, J.-L. Chen, X.-W. Han, J.-L. Zhang and S.-X. Yan, *J. Appl. Polym. Sci.*, 2015, **132**, 25.
38 E. S. Dragan, C. A. Gheorghita, M. V. Dinu, I. A. Duceac and S. Coseri, *Food Hydrocolloids*, 2023, **135**, 108147.
39 S. A. Kahdestani and M. H. Shahriari, *Abdouss, Polym. Bull.*, 2021, **78**, 1133–1148.
40 R. S. Devan and B. K. Chougule, *J. Appl. Phys.*, 2007, **101**(1), 014109.
41 X. Chen, E. Allahyarov, Q. Li, D. Langhe, M. Ponting, D. E. Schuele, E. Baer and L. Zhu, *Composites, Part B*, 2020, **190**, 107980.
42 D. Khare, B. Basu and A. Kumar Dubey, *Biomaterials*, 2020, **258**, 120280.
43 H. Birol, D. Damjanovic and N. Setter, *J. Am. Ceram. Soc.*, 2005, **88**, 1754–1759.
44 D. F. Crisler, J. J. Cupal and A. R. Moore, *Proc. IEEE*, 1968, **56**, 225–226.
45 J. Gomes, J. Nunes, V. Sencadas and S. L. Mendez, *Smart Mater. Struct.*, 2010, **19**, 065010.
46 E. Fukada, *Biorheology*, 1995, **32**, 593–609.
47 Y. Yang, S. Peng, F. Qi, J. Zan, G. Liu, Z. Zhao and C. Shuai, *Mater. Sci. Eng., C*, 2020, **116**, 111195.
48 C. Shuai, Z. Zeng, Y. Yang, F. Qi, S. Peng, W. Yang, C. He, G. Wang and G. Qian, *Mater. Des.*, 2020, **190**, 108564.
49 F. Qi, Z. Zeng, J. Yao, W. Cai, Z. Zhao and S. Peng, *Mater. Sci. Eng., C*, 2021, **126**, 112129.
50 B. Fana, Z. Guo, X. Li, S. Li, P. Gao, X. Xiao, J. Wu, C. Shen, Y. Jiao and W. Hou, *Bioact. Mater.*, 2020, **5**, 1087–1101.
51 D. L. Guzmán Sierra, I. Bdikin, A. Tkach, P. M. Vilarinho, C. Nunes and P. Ferreira, *Eur. J. Inorg. Chem.*, 2021, 792–803.
52 V. Melinte, A. L. Chibac-Scutaru, M. E. Culica and S. Coseri, *Appl. Surf. Sci.*, 2021, **565**, 150494.
53 S. Pongampai, T. Charoonsuk, N. Pinpru, P. Pulphol, W. Vittayakorn, P. Pakawanit and N. Vittayakorn, *Composites, Part B*, 2021, **208**, 10860.
54 E. Prokhorov, G. L. Bárcenas, B. L. Sánchez, B. Franc, F. Padilla-Vaca, M. Adelaido, H. Landaverde, J. M. Y. Limón and R. A. López, *Colloids Surf., B*, 2020, **196**, 111296.
55 A. Aassve, T. Capezzone, N. Cavalli, P. Conzo and C. Peng, *Sci. Rep.*, 2024, **14**(1), 1022.
56 R. Donate, R. Paz, R. Moriche, M. J. Sayagués, M. E. Alemán-Domínguez and M. Monzón, *Mater. Des.*, 2023, **231**, 112085.